Atmos. Chem. Phys. Discuss., doi:10.5194/acp-2016-219, 2016
Manuscript under review for journal Atmos. Chem. Phys.
Published: 18 April 2016

Atmospheric Chemistry and Physics Discussions

Vertical profiles of black carbon measured by a micro-aethalometer in summer in the North China Plain

L. Ran[1], Z. Z. Deng[1], X. B. Xu[2], P. Yan[3], W. L. Lin[3], Y. Wang[2], P. Tian[4], P. C. Wang[1], W. L. Pan[1], D. R. Lu[1]

[1]Key Laboratory of Middle Atmosphere and Global Environment Observation, Institute of Atmospheric Physics, Chinese Academy of Sciences, Beijing, 100029, China
[2]Key Laboratory for Atmospheric Chemistry, Institute of Atmospheric Composition, Chinese Academy of Meteorological Sciences, Beijing, 100081, China
[3]Meteorological Observation Center, China Meteorological Administration, Beijing, 100081, China
[4]Beijing Weather Modification Office, Beijing, 100089, China

Correspondence to: L. Ran (shirleyrl@mail.iap.ac.cn) and Z. Z. Deng (dengzz@mail.iap.ac.cn)

Abstract. Black carbon (BC) is a dominant absorber in visible spectrum and a potent factor in climatic effects. Vertical profiles of BC were measured using a micro-aethalometer attached to a tethered balloon during the Vertical Observations of trace Gases and Aerosols (VOGA) field campaign, in summer 2014 at a semirural site in the North China Plain (NCP). The diurnal cycle of BC vertical distributions following the evolution of the mixing layer was investigated for the first time in the NCP region. Statistical parameters including identified mixing height (H_m) and average mass concentrations within the mixing layer (C_m) and in free troposphere (C_f) were obtained for a selected dataset of 67 BC vertical profiles. H_m was usually lower than 0.2 km in the early morning and rapidly rose thereafter due to strengthened turbulence. The maximum height of the ML was reached in late afternoon. The top of a full developed ML exceeded 1 km on sunny days in summer, while stayed much lower on cloudy days. The sunset triggered the collapse of the ML and a stable nocturnal boundary layer (NBL) gradually formed. Accordingly, the highest level C_m was found in the early morning and the lowest in the afternoon. In the daytime, BC almost uniformly distributed within the ML and significantly decreased above the ML. During the field campaign, C_m averaged about 5.16±2.49 μg m^{-3}, with a range of 1.12 to 14.49 μg m^{-3}, comparable with observational results in many polluted urban areas. As evening approached, BC gradually built up near the surface and exponentially declined with height. In contrast to the large variability found both in H_m and C_m, C_f stayed relatively unaffected through the day. C_f was less than 10% of the ground level under clean conditions, while amounted to half of the ground level in some polluted cases. In-situ measurements of BC vertical profiles would hopefully have an important implication for accurately estimating direct radiative forcing by BC and improving the retrieval of aerosol optical properties by remote sensing in this region.

Atmos. Chem. Phys. Discuss., doi:10.5194/acp-2016-219, 2016
Manuscript under review for journal Atmos. Chem. Phys.
Published: 18 April 2016

Atmospheric Chemistry and Physics Discussions

1 Introduction

Black carbon (BC), produced from incomplete combustion processes, is a strongly absorbing constituent of atmospheric aerosols (Moosmüller et al., 2009; Bond et al., 2013). As a major absorber in the visible spectrum, BC heats the atmosphere and largely counterbalances cooling effects of scattering aerosols on climate (Jacobson, 2001; Ramanathan et al., 2005; Stier et al., 2007). Another reason for BC to be publicly concerned is that inhaled BC poses a huge threat to human health (Janssen et al., 2012; Nichols, 2013).

Despite the significance of evaluating radiative forcing by BC, large uncertainties arise from limitations of current knowledge on emissions, distributions and physical properties of BC (Andreae, 2001; Streets, et al., 2001; Bond et al., 2006; IPCC, 2013). One critical aspect pertinent to climate response of BC is a high sensitivity of BC radiative impact to its vertical distributions (Zarzycki and Bond, 2010; Ban-Weiss et al., 2012; Samset et al., 2013). The importance of BC vertical distributions to the evolution of planetary boundary layer (PBL) and cloud properties has also been demonstrated by previous studies (Yu et al., 2002; Ramanathan and Carmichael, 2008; Ferrero et al., 2014). Nevertheless, vertical profiles of BC or aerosol absorption have only been scarcely measured in a few field campaigns (Safai et al., 2012 and references therein; Ryerson et al., 2013). Available information on BC vertical distributions are particularly limited in China (Zhang et al., 2012; Li et al., 2015; Zhao et al., 2015), issuing a challenge to reliably estimate regional climatic effects of BC under severe air pollution due to rapid economic growth and urbanization in this region (Menon et al., 2002; Liao and Shang, 2015 and references therein).

Platforms normally utilized to perform BC profiling are tethered balloons, aircrafts and unmanned aerial vehicles. BC vertical profiles obtained from in-situ measurements using tethered balloons are highly vertically-resolved, revealing details within about 1 km above the ground, especially in the thin surface layer that is vital for human beings and where various sources are located (Ferrero et al., 2011a, Babu et al., 2011a; Li et al., 2015). Comparatively, aircrafts (Tripathi et al., 2005, 2007; Metcalf et al., 2012; Zhao et al., 2015) and unmanned aerial vehicles (Corrigan et al., 2008; Höpner et al., 2016) are more expensive, although they have advantages of reaching higher altitudes and for aircrafts more onboard instruments in the size and weight unable to be carried by tethered balloons and unmanned aerial vehicles. Fast flight speeds of these two platforms also compromise their spatial resolutions. In addition, high altitude balloon was employed to measure BC vertical profiles at high altitudes in free troposphere, e. g., two BC polluted layers found at about 4.5 km and 8 km altitudes were reported by Babu et al. (2011b). Indirect methods such as recently proposed Lidar remote sensing might be able to conduct continuous measurements (Miffre et al., 2015), they are however less accurate than in-situ measurements.

To advance understanding in impacts of atmospheric components including trace gases and aerosols on atmospheric environment and climate, an intensive field campaign, Vertical Observations of trace Gases and Aerosols (VOGA), was carried out in summer 2014 at a semirural site in the North China Plain (NCP), one of the most overcrowded and polluted regions in the world (Shao et al., 2006; Xu et al., 2011; Ma et al., 2011; Chen et al., 2012). A tethered balloon system equipped with instruments was employed for high vertical resolution measurements within 1 km above the ground. In this

Atmos. Chem. Phys. Discuss., doi:10.5194/acp-2016-219, 2016
Manuscript under review for journal Atmos. Chem. Phys.
Published: 18 April 2016

Atmospheric Chemistry and Physics Discussions

study, we present results from in-situ measurements of BC vertical profiles using a lightweight (about 280 g) and small-sized (117 mm×66 mm×38 mm) micro-aethalometer (microAeth® Model AE-51, Magee Scientific, USA). The diurnal cycle of BC vertical distributions was explored for the first time in the NCP region.

2 Experiment

The VOGA 2014 field campaign was carried out in the period from June 21 to July 14 at a semirural site Raoyang (38.14°N, 115.44°E, 20 m a.s.l.), about 50 km north of the city of Hengshui in the central NCP as shown in Fig. 1 in Ran et al. (2016). The county of Raoyang, in which the site is located, is less industrialized and relies mainly on agriculture, but surrounded by a cluster of industrial and populated cities within a distance of 100 km, and respectively about 190 km and 160 km southwest of the twin megacities of Beijing and Tianjin.

2.1 Instruments

A micro-aethalometer to measure aerosol absorption at 880 nm and a radiosonde to measure meteorological parameters (pressure, temperature, relative humidity, wind speed and direction) were attached to a helium-filled tethered balloon, with a volume of 30 m^3 and a payload weight of 10 kg. The fish-shaped balloon was well balanced during launches, thus the disturbance imposed on instruments by ascents and descents of the balloon could be largely minimized. Launches were scheduled every 3 hours between 06:00 and 21:00 (Local Time, LT) from the ground to 1 km height. However, feasible launches actually depended upon wind speeds and the precipitation, as well as air traffic control. In total, 48 successful launches were conducted on 15 days, of which 40 reached above 0.5 km. Through the entire field campaign, 89 vertical profiles of BC were reliably obtained. Lack of data for several ascending or descending processes was primarily caused by wind gusts, which led to destabilization of the tethered balloon and poor data quality. The balloon ascended at a rate of 1 m/s and descended at a rate of 0.5 m/s under the control of an electric winch. With a sampling interval of 1 s for all instruments, the observational vertical resolution was ~1 m. For analysis in this study, 20-m averaged data were used.

AE-51 operated with a similar principle of the aethalometer as described in Hansen et al. (1984). The intensity of transmitted light through a 3-mm diameter sample spot (I) and an aerosol-free reference spot (I_0) on a T60 Teflon-coated borosilicate glass fiber filter were simultaneously detected to estimate aerosol absorption coefficients at the wavelength of 880 nm following:

$$\sigma_{\text{AE-51,880nm}} = \frac{A \times \Delta\text{ATN}}{100 \times F \times \Delta t}, \quad (1)$$

where A is the area of the aerosol collecting spot (0.071 cm^2), F is the flow rate (150 ml min^{-1}), ATN denotes light attenuation and calculated from $100\times\ln(I_0/I)$, ΔATN is the change of ATN during the sampling interval Δt (1 s). A homemade silica gel dryer was placed in front of the inlet to efficiently dry ambient aerosols. A test on the dryer was performed before the campaign to ensure the duration and efficiency of its usage.

Atmos. Chem. Phys. Discuss., doi:10.5194/acp-2016-219, 2016
Manuscript under review for journal Atmos. Chem. Phys.
Published: 18 April 2016

Atmospheric Chemistry and Physics Discussions

2.2 Data processing

2.2.1 Smoothing algorithm

At a high temporal resolution of 1 s, steady increase of ATN with sampling time was not as usually found due to instrumental noises. Acquired data was consisted of many large values with positive or negative signs. A post-processing method, Optimized Noise-reduction Averaging (ONA) algorithm, has been developed by Hagler et al. (2011), where adaptive time-averaging of the BC data was conducted with the time window of averaging optimally chosen by ΔATN. In this study, data dispersion due to high temporal resolution was treated by a new smoothing algorithm. The procedure was performed as following:

(1) For each data point x_i of a continuously measured time series with N records, calculate the difference between x_i and all other data points within n seconds to generate a matrix of $D_{i,j}=|x_i-x_{i+j}|$, where $i=1,2,\ldots,N\text{-}1,N$ and $j=-n,-n+1,\ldots,n\text{-}1,n$;

(2) Find the largest value of the matrix $D_{k,l}$, which is the difference between point x_k and x_{k+l};

(3) Replace x_k and x_{k+l} with $(x_k+x_{k+l})/2$ and set $D_{k,l}$ to a minus number;

(4) Replace any $D_{i,j}$ that has been calculated using x_k or x_{k+l}, except for $D_{i,j}$ with a minus number. This step is optional, since it largely raises the computational cost;

(5) Repeat step (2)-(4) until no positive numbers in the matrix;

(6) Repeat step (1)-(5) for m times to obtain acceptable smoothed data.

It should be kept in mind that using improper large smoothing window n or smoothing count m might wipe off some natural variations, although it will always give a smoother result. n should be set to no more than 5, given that data fluctuations are normally already compensated within 5 s. The smoothing count m is set to be 5 in this study. A comparison made between smoothed data using our algorithm and the method in Hagler et al. (2011) indicated that our procedure reduced more fluctuations and kept reasonable variations of the data.

2.2.2 Correction of absorption coefficients

Measured $\sigma_{AE\text{-}51,880nm}$ suffered from systematic biases inherent in the filter-based technique, including an underestimation due to loading effect and an overestimation due to aerosol scattering and multiple scattering of filter fibers (Weingartner et al., 2003; Arnott et al., 2005; Schmid et al., 2006; Collaud Coen et al., 2010). With a new filter for each launch, loading effect, a saturation-induced reduction in the optical path along with increasing aerosol loading, could be neglected in this study. Hence, mass concentrations of BC (m_{BC}) could be directly converted from $\sigma_{AE\text{-}51,880nm}$ using the documented 'specific attenuation' of 12.5 ($m^2\ g^{-1}$), considering that BC is the major contributor to aerosol absorption at 880 nm (Ramachandran and Rajesh, 2007).

The determination of BC absorption coefficients (σ_{BC}) from $\sigma_{AE\text{-}51,880nm}$ required a correction for aerosol scattering and multiple scattering of filter fibers. The correction factor (C) used to correct these artifacts was derived on basis of a 1-week surface comparative test in Beijing among AE-51, a 7-wavelength aethalometer (Model AE-31, Magee Scientific, USA) and

Atmos. Chem. Phys. Discuss., doi:10.5194/acp-2016-219, 2016
Manuscript under review for journal Atmos. Chem. Phys.
Published: 18 April 2016

Atmospheric Chemistry and Physics Discussions

a multi-angle absorption photometer (MAAP, Model 5012, Thermo, USA). Aerosol absorption coefficients at 670 nm ($\sigma_{MAAP,670nm}$) were measured by MAAP. Multi-angle detections of the transmittance and reflectance, as well as a two-stream approximation in the radiative transfer scheme adopted by MAAP have significantly improved measurements of ambient aerosol absorption coefficients (Petzold and Schönlinner, 2004; Petzold et al., 2005). Thereby, $\sigma_{MAAP,670nm}$ were taken as real values for subsequent corrections. Aerosol absorption Angström exponent (α) needed for estimating $\sigma_{MAAP,880nm}$ was calculated from absorption coefficients at 660 nm ($\sigma_{AE\text{-}31,660}$) and 880 nm ($\sigma_{AE\text{-}31,880}$), which were corrected from measurements of AE-31:

$$\alpha = \frac{\ln(\sigma_{AE\text{-}31,660nm}) - \ln(\sigma_{AE\text{-}31,880nm})}{\ln(880) - \ln(660)}. \quad (2)$$

Details of the correction scheme developed for tackling with artifacts of AE-31 were described in Ran et al. (2016). Following the spectral dependence of aerosol absorption coefficients in the form of $\lambda^{-\alpha}$, $\sigma_{MAAP,880nm}$ could be quantified from $\sigma_{MAAP,670nm}$ by:

$$\sigma_{MAAP,880nm} = \sigma_{MAAP,670nm} \times (\frac{880}{670})^{-\alpha}, \quad (3)$$

Measured $\sigma_{AE\text{-}51,880nm}$ (ATN<10) and calculated $\sigma_{MAAP,880nm}$ were linearly fitted with a correlation coefficient of 0.96 in a significant level (P<0.001), yielding a C value of 2.52. By dividing C into $\sigma_{AE\text{-}51,880nm}$, absorption coefficients σ_{BC} could be estimated.

2.2.3 Calculation of meteorological parameters

Instead of measured temperature (T) and relative humidity (RH), two conservative quantities, potential temperature (θ) and specific humidity (q) were used to provide information on the evolution of PBL. The calculation of θ (K) followed:

$$\theta = T \times \left(p_0 / p \right)^{R_d / C_{pd}}, \quad (4)$$

where p and p_0 are respectively measured pressure and the standard pressure at the sea level (hPa), T is measured temperature (K), R_d is the individual gas constant for dry air (287 J kg^{-1} K^{-1}), C_{pd} is the specific heat at constant pressure for dry air at the standard temperature (1005 J kg^{-1} K^{-1}). Calculated θ was then expressed in degree Celsius (^{o}C) in order to be straightforward. Specific humidity (q, g kg^{-1}) was calculated from:

$$q = \varepsilon \times \frac{e}{p - (1-\varepsilon) \times e} \times 1000, \quad (5)$$

where ε is the ratio of the molecular weight of water vapour to that of dry air (0.622), e is the vapour pressure of water (hPa), which is the product of measured RH (%) and calculated water saturation pressure (e_s) at each measured temperature T.

3 Results and Discussion

3.1 Vertical distributions of BC and meteorological parameters

Atmos. Chem. Phys. Discuss., doi:10.5194/acp-2016-219, 2016
Manuscript under review for journal Atmos. Chem. Phys.
Published: 18 April 2016

Atmospheric Chemistry and Physics Discussions

A set of 67 vertical profiles of BC and meteorological parameters were selected. The mixing layer (ML) could be clearly discerned for profiles measured in the daytime. Exceptions were those measured around noon, when the top of the ML, often higher than 1 km in summer, was beyond reach of the tethered balloon. In addition, several launches took place in the evening to observe BC vertical distributions shaped by the nocturnal boundary layer (NBL). A statistical summary of the field campaign and the meteorology is given in Table 1. Most profiles were sampled under mild winds in the morning and evening, when relatively stable conditions suitable for launches of the tethered balloon were more easily encountered. Air masses were mainly carried, either by southeasterly or southwesterly winds, from areas densely populated and heavily industrialized, also ramified with railways and highroads.

Figure 1 illustrates an example of vertical distributions of BC, θ, q, and winds during one launch on July 8, 2014 (10:41-11:27 LT). 20-m averaged data are denoted by dots in dark color for the ascent and light color for the descent. Arrows depict vector mean horizontal winds, with the length to represent wind speed and the arrowhead to give wind direction following meteorological definitions. The height of a clearly defined ML (H_m) was marked by a solid line for each BC vertical profile. H_m was calculated from a sigmoid function that could well characterize typical daytime profile of m_{BC}:

$$m_{BC} = C_{ms} - \frac{C_{ms} - C_{fs}}{e^{-(h-H_m)/H_e} + 1} \quad (6)$$

where C_{ms} and C_{fs} are respectively characteristic m_{BC} within the ML and in the free troposphere (FT), H_e represents the thickness of the entrainment layer (EL), h is the height at which each 20-m averaged m_{BC} is obtained. H_m determined from profiles of θ and q generally agreed well with that from profiles of m_{BC}. The reliability of estimating H_m from vertical measurements of BC had also been demonstrated in previous studies (Ferrero et al., 2010; Ferrero et al., 2011b). A nearly uniform distribution of BC, as well as θ and q, was observed within the strongly convective ML. Large vertical gradient of m_{BC} across EL led to approximately 50% reduction from the level in the ML to that in FT. Concomitantly, a substantial reduction in q, whereas an increase in θ, was also immediately found above the ML. The difference in profiles between the ascent and the descent evidently indicated a rapid evolution of the ML near noon and its impact on vertical distributions of BC and meteorology. More discussions regarding diurnal variations of BC vertical profiles will be found in next section.

Table 2 summaries calculated parameters for BC vertical profiles during different periods. Average m_{BC} within the ML and in the FT were denoted as C_m and C_f, which were C_{ms} and C_{fs} for typical BC vertical profiles. As for non-typical BC vertical profiles, either as a result of a polluted layer in FT or barely sufficient height into FT reached by the tethered balloon, a sigmoid function was not applicable and the gradient method was used to estimate H_m (Seibert et al., 2000; Kim, et al., 2007). C_m was the average value of m_{BC} below H_m. Near sunset, the NBL forms along with the collapse of the ML (Kaimal and Finnigan, 1994; Larzridis, 2011). The structure of the NBL is more complicated and the determination of the NBL height bears more uncertainty (Yu, 1978; Poulos, et al., 2002). A subjective procedure based on the gradient method was utilized to estimate the NBL height, which was also denoted as H_m in this study for convenience. Only C_f was obtained from averaging m_{BC} above H_m for such cases. H_m could not be determined when exceeding 1 km as above stated. Under such circumstance, m_{BC} measured along the ascending/descending path from the ground to the maximum height reached by the tethered balloon

Atmos. Chem. Phys. Discuss., doi:10.5194/acp-2016-219, 2016
Manuscript under review for journal Atmos. Chem. Phys.
Published: 18 April 2016

Atmospheric Chemistry and Physics Discussions

were averaged to obtain C_m. A large variability was found in C_m, with a range of 1.12 to 14.49 μg m^{-3}. On average, C_f stayed relatively steadily, though it ranged from 0.36 μg m^{-3} in clean cases to 3.14 μg m^{-3} under polluted conditions.

Statistically, vertical profiles of BC were categorized into two types, according to their shapes along the normalized height (H_{Nor}), which was calculated from h/H_m-1. H_{Nor} shows the surface with a value of -1 and the top of the ML with a value of 0. One type of BC vertical profiles, exclusively measured in the daytime, displayed a vertical distribution typically shaped by a well-mixed mixing layer (Fig. 2a). BC almost uniformly distributed within the ML, in a similar way as the example (Fig. 1), with an average m_{BC} level of about 5.16±2.49 μg m^{-3}, or σ_{BC} of about 25.60±12.35 Mm^{-1}. This is comparable with what has been observed within the PBL in many polluted urban areas (Table 3). A couple of highly polluted cases, where C_m exceeded 10 μg m^{-3}, were observed in the early morning. The formation of the convective ML just started at that time and vertical turbulence was yet not strong enough to dilute the high level of BC, which was primarily emitted near the ground and accumulated within the stable NBL over night. Due to a sharp reduction in m_{BC} from the ML to FT, average C_f was about 1.61±0.94 μg m^{-3}. The second type of BC vertical profiles revealed the feature of trapped air pollutants in the shallow stable NBL. m_{BC} nearly exponentially declined with H_{Nor}, as a result of weakened turbulence and vertical dispersion. Under polluted conditions, C_f could reach as high as 2.83 μg m^{-3}, otherwise usually well below 1μg m^{-3}.

3.2 Diurnal variations of BC vertical profiles

An investigation on diurnal variations of BC vertical profiles was able to be undertaken on July 1, 8, and 13, when measurements generally covered the period from early morning to afternoon or evening. On other observational days, the dataset was incomplete due to aborted launches under strong winds or precipitation. For clarity, only the vertical profile during the descent of each launch is plotted in Fig. 3. Additionally, profiles not included into the selected dataset are also shown.

A distinct diurnal variation was found both in the shape of BC vertical profiles and the level of m_{BC} along the profile. To a great extent, the diurnal cycle of BC vertical profiles followed the evolution of the ML. In the early morning, BC was largely restricted within a thin ML less than 200 m above the ground when vertical turbulence was still weak. m_{BC} dropped dramatically from a high level within the ML to a significantly low level above the ML, even less than 10% as could be found on July 13. In polluted cases, however, m_{BC} in FT could exceed 2 μg m^{-3} and sometimes reach nearly 50% of that at the surface (e.g., profiles on July 8). Gradually, vertical turbulence in the ML strengthened as the earth was continuously heated by solar radiation after sunrise. The convective ML developed quickly in the forenoon, with elevated H_m and decreased C_m. Marked changes in BC vertical profiles could be observed even during one launch when the mixing height rose so rapidly, as shown in the example (Fig. 1). The maximum height of the ML commonly exceeded 1 km in the afternoon during the field campaign (e.g., profiles on July 8), except on cloudy days when the ML did not fully develop. As the evening approached, convection abruptly decayed and a stable NBL began to form. m_{BC} in FT promptly declined to its typical level, often leaving no trail to indicate the daytime mixing with polluted air masses beneath. In contrast, air pollutants including BC quickly built up in the shallow NBL.

Atmos. Chem. Phys. Discuss., doi:10.5194/acp-2016-219, 2016
Manuscript under review for journal Atmos. Chem. Phys.
Published: 18 April 2016

Atmospheric Chemistry and Physics Discussions

It was interestingly noticed that a polluted layer with a thickness of about 0.3 km, extending from the height of 0.2 km to 0.5 km, lay right above the ML in the early morning on July 1. The polluted layer could also be accordingly recognized from meteorological features of more moisture and wind shear across its boundaries. Wind direction was southeast in the ML and FT, while southwest in the polluted layer. Average m_{BC} within the polluted layer was about 4 μg m^{-3}, half of that near the surface and double of that in FT. Actually, the vertical profile within the morning ML quite resembled characteristics of a nocturnal profile even though the sun had risen, suggesting that strong inversion of the NBL still overrode weak vertical turbulence at that time. As surface emissions from human activities kept increasing, m_{BC} within the ML elevated. Further development of vertical convection broke the layered structure, leading to the merge of the polluted layer and the ML. Slowly, the polluted layer vanished into the convective ML, though remained until 9:00 LT in the morning. An elevated aerosol layer (0.7~1 km), in which BC was well aged, has previously been observed in the afternoon over Beijing by Zhang et al. (2012), and was attributed to the residual nocturnal stable layer. Possible origin of the polluted layer present here and the status of BC in the layer were unable to be decided on basis of limited observations. Nonetheless, a higher q in the polluted layer than at the surface and different wind direction might imply an elevated residual layer formed after sunset on the day before and transported from somewhere else. It was quite cloudy and sultry during the daytime, and a heavy rainfall occurred near the evening. Thus, the top of the ML was still below 0.5 km when the launch was carried out around noon. Despite that the tethered balloon failed to reach 1 km due to strong winds aloft, a part of a relatively polluted layer with apparent increase in moisture and potential temperature could be roughly distinguished. Wind direction in the polluted layer was southwest, whereas predominant wind direction beneath had changed to southeast. The polluted layer, extending from about 0.7 m to the top of the reachable height, disappeared during the last launch around 14:00 LT on that day and was probably a transported plume.

Figure 4 displays H_m and m_{BC} from the entire selected dataset on a diurnal scale. Observations on each day are shown in one color. Variations in H_m through the field campaign generally resembled the diurnal cycle observed on an individual day (Fig. 4a). The ML, though still shallow, developed slowly after sunrise. In addition to a high level of BC trapped near the ground by the stable NBL, fresh emissions from daytime human activities further aggravated surface pollution. Observed m_{BC} was usually quite high in the early morning, sometimes even experienced an increase with time, depending upon how fast the ML developed and emissions increased. The thickening of the mixing depth accelerated in late morning on sunny days, whereas impeded on cloudy days only to form a thin mixing layer. Accordingly, C_m (solid dots in Fig. 4b) largely reduced from morning to noon in strongly convective ML on sunny days, however, stayed relatively stable through morning on cloudy days. Comparative cases could be found on July 1 and 14. Based on current knowledge of the boundary layer, the maximum height of the ML on sunny days would be reached in late afternoon, but could not be observed in this study since it was well above the flight limit of the tethered balloon. The collapse of the ML was not directly captured. However, intensive measurements favored by the meteorology on July 8 revealed that the convective ML quickly faded away on a time scale of 1 hour near sunset. Instead, a stable and shallow NBL confined nighttime emissions near the ground, giving rise to enhanced surface pollution (open dots in Fig. 4b).

Atmos. Chem. Phys. Discuss., doi:10.5194/acp-2016-219, 2016
Manuscript under review for journal Atmos. Chem. Phys.
Published: 18 April 2016

Atmospheric Chemistry and Physics Discussions

4 Conclusions

In-situ measurements of black carbon (BC) vertical profiles were carried out at a semirural site during the VOGA 2014 summer field campaign, using a micro-aethalometer attached to a tethered balloon system. A set of 67 BC vertical profiles was reliably collected and diurnal variations of BC vertical profiles were examined.

Vertical distributions of BC and meteorological parameters, as well as the mixing height (H_m) identified from BC profiles, experienced a distinct diurnal cycle guided by the development of the mixing layer (ML). In the morning, weak turbulence within the shallow ML (thinner than 0.2 km) favored the accumulation of enhanced surface emissions, sometimes leading to a severe pollution with BC mass concentrations (m_{BC}) exceeding 10 μg m^{-3}. The high level of BC within the ML was diluted with the fast development of a strongly convective ML. H_m reached its maximum in late afternoon and exceeded 1 km on sunny days, whereas stayed much lower on cloudy days. Typically in the daytime, BC uniformly distributed within the ML and sharply decreased above the ML to a level even less than 10% of that near the surface. Average m_{BC} within the ML (C_m) was about 5.16±2.49 μg m^{-3} over the entire field campaign, with a range of 1.12 to 14.49 μg m^{-3}, comparable with what has been observed in many polluted urban areas. C_f, average m_{BC} in free troposphere (FT), was below 1μg m^{-3} under clean conditions and amounted to half of the ground level under pollution conditions. In the evening, BC quickly built up near the surface and exponentially declined with height, following the collapse of the ML and the formation of a stable nocturnal boundary layer (NBL). Particularly, two polluted layers were observed at different time and heights on July 1. Origins of the polluted layers were not able to be evidently decided. However, the presence of BC polluted layers in FT, either as an elevated residual layer in the morning or a transported plume in the afternoon as suggested by the history of the layer and the meteorology, might considerably influence direct radiative forcing by BC and atmospheric stability.

Acknowledgements

This research was funded by the National Natural Science Foundation of China (NSFC) under Grant No. 41305114, 41205098, 41330442 and 41127901. This work was also supported by China Special Fund for Meteorological Research in the Public Interest (No. GYHY201206015). We are grateful to Yong Wang, Chuncheng Ji, Qihua Du, Hanze Yu and Xinpan Li for their cooperation in launching the tethered balloon. We also thank Raoyang Meteorological Bureau for providing the location for our measurements.

Appendix A Nomenclature Table

Symbol	Definition
α	Aerosol absorption Angström exponent, here calculated from $\sigma_{AE\text{-}31,660nm}$ and $\sigma_{AE\text{-}31,880nm}$
$\sigma_{AE\text{-}31,660nm}$	Aerosol absorption coefficient measured by AE-31 at the wavelength of 660 nm

Atmos. Chem. Phys. Discuss., doi:10.5194/acp-2016-219, 2016
Manuscript under review for journal Atmos. Chem. Phys.
Published: 18 April 2016

$\sigma_{AE\text{-}31,880nm}$	Aerosol absorption coefficient measured by AE-31 at the wavelength of 880 nm
$\sigma_{MAAP,670nm}$	Aerosol absorption coefficient measured by MAAP at the wavelength of 670 nm
$\sigma_{MAAP,880nm}$	Aerosol absorption coefficient at the wavelength of 880 nm, calculated from α and $\sigma_{MAAP,670nm}$
$\sigma_{AE\text{-}51,880nm}$	Aerosol absorption coefficient measured by AE-51 at the wavelength of 880 nm
σ_{BC}	Absorption coefficient of black carbon at the wavelength of 880 nm
λ	Wavelength
θ	Potential temperature
ATN	Light attenuation
C	Correction factor for filter multiple scattering and aerosol scattering
C_f	Average m_{BC} in the free troposphere
C_m	Average m_{BC} within the mixing layer
C_{fs}	Characteristic m_{BC} in the free troposphere, derived from sigmoid fitting
C_{ms}	Characteristic m_{BC} within the mixing layer, derived from sigmoid fitting
H_e	The thickness of the entrainment layer, derived from sigmoid fitting
H_m	The height of the mixing layer
H_{Nor}	The normalized height, defined as h/H_m-1
m_{BC}	Mass concentration of black carbon, converted from $\sigma_{AE\text{-}51,880nm}$
q	Specific humidity
RH	Relative humidity
T	Temperature

References

Andreae, M. O.: The dark side of aerosols, Nature, 409, 671-672, 2001.

Arnott, W. P., Hamasha, K., Moosmuller, H., Sheridan P. J., and Ogren J. A.: Towards aerosol light-absorption measurements with a 7-wavelength aethalometer: evaluation with a photoacoustic instrument and 3-wavelength nephelometer, Aerosol Sci. Tech., 39, 17-29, doi: 10.1080/027868290901972, 2005.

Babu, S. S., Sreekanth, V., Moorthy, K. K., Mohan, M., Kirankumar, N. V. P., Subrahamanyam, D. B., Gogoi, M. M., Kompalli, S. K., Beegum, N., Chaubey, J. P., Kumar, V. H. A., and Manchanda, R. K.: Vertical profiles of aerosol black carbon in the atmospheric boundary layer over a tropical coastal station: Perturbations during an annular solar eclipse, Atmos. Res., 99. 471-478, doi:10.1016/j.atmosres.2010.11.019, 2011a.

Babu, S. S., Moorthy, K. K., Manchanda, R. K., Sinha, P. R., Satheesh, S. K., Vajja, D. P., Srinivasan, S., and Kumar, V. H.

A.: Free tropospheric black carbon aerosol measurements using high altitude balloon: Do BC layers build "their own homes" up in the atmosphere?, Geophys. Res. Lett., 38, L08803, doi:10.1029/2011GL046654, 2011b.

Ban-Weiss, G. A., Cao, L., Bala, G., and Caldeira, K.: Dependence of climate forcing and response on the altitude of black carbon aerosols, Clim. Dyn., 38, 897-911, doi:10.1007/s00382-011-1052-y, 2012.

Bond, T. C., Habib, G., Bergstrom, R. W.: Limitations in the enhancement of visible light absorption due to mixing state, J. Geophys. Res., 111, D20211, doi:10.1029/2006JD007315, 2006.

Bond, T. C., Doherty, S. J., Fahey, D. W., Forster, P. M., Berntsen, T., DeAngelo, B. J., Flanner, M. G., Ghan, S., Kärcher, B., Koch, D., Kinne, S., Kondo, Y., Quinn, P. K., Sarofim, M. C., Schultz, M. G., Schulz, M., Venkataraman, C., Zhang, H., Zhang, S., Bellouin, N., Guttikunda, S. K., Hopke, P. K., Jacobson, M. Z., Kaiser, J. W., Klimont, Z., Lohmann, U., Schwarz, J. P., Shindell, D., Storelvmo, T., Warren, S. G., and Zender, C. S.: Bounding the role of black carbon in the climate system: a scientific assessment, J. Geophys. Res., 118, 5380-5552, doi:10.1002/jgrd.50171, 2013.

Chen, J., Zhao, C. S., Ma, N., Liu, P. F., Göbel, T., Hallbauer, E., Deng, Z. Z., Ran, L., Xu, W. Y., Liang, Z., Liu, H. J., Yan, P., Zhou, X. J., and Wiedensohler, A.: A parameterization of low visibilities for hazy days in the North China Plain, Atmos. Chem. Phys., 12, 4935-4950, doi:10.5194/acp-12-4935-2012, 2012.

Collaud Coen, M., Weingartner, E., Apituley, A., Ceburnis, D., Fierz-Schmidhauser, R., Flentje, H., Henzing, J. S., Jennings, S. G., Moerman, M., Petzold, A., Schmid, O., and Baltensperger, U.: Minimizing light absorption measurement artifacts of the aethalometer: evaluation of five correction algorithms, Atmos. Meas. Tech., 3, 457-474, doi:10.5194/amt-3-457-2010, 2010.

Corrigan, C. E., Roberts, G. C., Ramana, M. V., Kim, D., and Ramanathan, V.: Capturing vertical profiles of aerosols and black carbon over the Indian Ocean using autonomous unmanned aerial vehicles, Atmos. Chem. Phys., 8, 737-747, doi:10.5194/acp-8-737-2008, 2008.

Ferrero, L., Perrone, M. G., Petraccone, S., Sangiorgi, G., Ferrini, B. S., Lo Porto, C., Lazzati, Z., Cocchi, D., Bruno, F., Greco, F., Riccio, A., and Bolzacchini, E.: Vertically-resolved particle size distribution within and above the mixing layer over the Milan metropolitan area, Atmos. Chem. Phys., 10, 3915-3932, doi:10.5194/acp-10-3915-2010, 2010.

Ferrero, L., Mocnik, G., Ferrini, B. S., Perrone, M. G., Sangiorgi, G., and Bolzacchini, E.: Vertical profiles of aerosol absorption coefficient from micro-aethalometer data and Mie calculation over Milan, Sci. Total Environ., 40, 2824-2837, doi:10.1016/j.scitotenv.2011.04.022, 2011a.

Ferrero, L., Riccio, A., Perrone, M. G., Sangiorgi, G., Ferrini, B. S., and Bolzacchini, E.: Mixing height determination by tethered balloon-based particle soundings and modeling simulations, Atmos. Res., 102, 145-156, doi:10.1016/j.atmosres.2011.06.016, 2011b.

Ferrero, L., Castelli, M., Ferrini, B. S., Moscatelli, M., Perrone, M. G., Sangiorgi, G., D'Angelo, L., Rovelli, G., Moroni, B., Scardazza, F., Mocnik, G., Bolzacchini, E., Petitta, M., and Cappelletti, D.: Impact of black carbon aerosol over Italian basin valleys: high-resolution measurements along vertical profiles, radiative forcing and heating rate, Atmos. Chem. Phys., 14, 9641-9664, doi:10.5194/acp-14-9641-2014, 2014.

Hagler, G. S. W., Yelverton, T. L. B., Vedantham, R., Hansen, A. D. A. and Turner, J. R.: Post-Processing Method to Reduce Noise while Preserving High Time Resolution in Aethalometer Real-Time Black Carbon Data, Aerosol Air Qual. Res., 11, 539-546, 2011.

Hansen, A. D. A., Rosen, H., and Novakov, T.: The aethalometer - an instrument for the real-time measurement of optical absorption by aerosol particles, Sci. Total Environ., 36, 191-196, 1984.

Höpner, F., Bender, F. A. M., Ekman, A. M. L., Praveen, P. S., Bosch, C., Ogren, J. A., Andersson, A., Gustafsson, Ö. And Ramanathan, V.: Vertical profiles of optical and microphysical particle properties above the northern Indian Ocean during CARDEX 2012, Atmos. Chem. Phys., 16, 1045-1064, doi:10.5194/acp-16-1045-2016, 2016.

IPCC: Summary for policymakers. Climate change 2013: the physical science basis, Cambridge University Press, Cambridge, UK and New York, NY, USA, 2216 pp, 2013.

Jacobson, M. Z.: Strong radiative heating due to the mixing state of black carbon in atmospheric aerosols, Nature, 409, 695-697, 2001.

Janssen, N. A., Gerlofs-Nijland, M. E., Lanki, T., Salonen, R. O., Cassee, F., Hoek, G., Fischer, P., Brunekreef, B., and Krzyzanowski, M.: Health effects of black carbon, World Health Organization, Copenhagen, 2012.

Kaimal, J. C., and Finnigan, J. J.: Atmospheric boundary layer flows: their structure and measurement, Oxford University Press, New York, 289 pp., 1994.

Kim, S. W., Yoon, S. C., Won, J. G., and Choi, S. C.: Ground-based remote sensing measurements of aerosol and ozone in an urban area: a case study of mixing height evolution and its effect on ground-level ozone concentrations, Atmos. Environ., 41, 7069-7081, 2007.

Lazaridis, M.: First principles of meteorology and air pollution, Environ. Poll., Springer Netherlands, 362 pp., 2010.

Li, J., Fu, Q. Y., Huo, J. T., Wang, D. F., Yang, W., Bian, Q. G., Duan, Y. S., Zhang, Y. H., Pan, J., Lin, Y. F., Huang, K., Bai, Z. P., Wang, S. H., Fu, J. S., and Louie, P. K. K.: Tethered balloon-based black carbon profiles within the lower troposphere of Shanghai in the 2013 East China smog, Atmos. Environ., 123, 327-338, doi:10.1016/j.atmosenv.2015.08.096, 2015.

Liao, H., and Shang, J. J.: Regional warming by black carbon and tropospheric ozone: a review of progresses and research challenges in China, J. Meteor. Res., 29, 525-545, doi:10.1007/s13351-015-4120-0, 2015.

Ma, N., Zhao, C. S., Nowak, A., Müller, T., Pfeifer, S., Cheng, Y. F., Deng, Z.Z., Liu, P. F., Xu, W. Y., Ran, L., Yan, P., Göbel, T., Hallbauer, E., Mildenberger, K., Henning, S., Yu, J., Chen, L. L., Zhou, X. J., Stratmann, F., and Wiedensohler, A.: Aerosol optical properties in the North China Plain during HaChi campaign: an in-situ optical closure study, Atmos. Chem. Phys., 11, 5959-5973, doi:10.5194/acp-11-5959-2011, 2011.

Menon, S., Hansen, J., Nazarenko, L., Luo, Y. F.: Climate effects of black carbon aerosols in China and India, Science, 297, doi:10.1126/science.1075159, 2250-2253, 2002.

Metcalf, A. R., Craven, J. S., Ensberg, J. J., Brioude, J., Angevine, W., Sorooshian, A., Duong, H. T., Jonsson, H. H., Flagan, R. C., Seinfeld, J. H.: Black carbon aerosol over the Los Angeles Basin during CalNex, J. Geophys. Res., 117, D00V13, doi:10.1029/2011JD017255, 2012.

Miffre, A., Anselmo, C., Geffroy, S., Frejafon, E., and Rairoux, P.: Lidar remote sensing of laser-induced incandescence on light absorbing particles in the atmosphere, Opt. Exp., 23, 2347-2360, doi:10.1364/OE.23.002347, 2015.

Moosmüller, H., Chakrabarty, R. K., and Arnott, W. P.: Aerosol light absorption and its measurement: a review, J. Quant. Spectrosc. Radiat. Transfer, 110, 844-878, doi:10.1016/j.jqsrt.2009.02.035, 2009.

Nichols, J. L., Owens, E. O., Dutton, S. J., and Luben, T. J.: Systematic review of the effects of black carbon on cardiovascular, Int. J. Public Health, 58, 707-724, doi:10.1007/s00038-013-0492-z, 2013.

Petzold, A., and Schönlinner, M.: Multi-angle absorption photometry - a new method for the measurement of aerosol light absorption and atmospheric black carbon, J. Aerosol Sci., 35, 421-441, doi:10.1016/j.jaerosci.2003.09.005, 2004.

Petzold, A., Schloesser, H., Sheridan, P. J., Arnott, W. P., Ogren, J. A., and Virkkula, A.: Evaluation of multiangle absorption photometry for measuring aerosol light absorption, Aerosol Sci. Technol., 39, 40-51, doi: 10.1080/027868290901945, 2005.

Poulos, G. S., Blumen, W., Fritts, D. C., Lundquist, J. K., Sun, J. L., Burns, S. P., Nappo, C., Banta, R., Newsom, R., Cuxart, J., Terrandellas, E., Balsley, B., and Jensen, M.: CASES-99: a comprehensive investigation of the stable nocturnal boundary layer, Bull. Am. Meteorol. Soc., 83, 555-581, 2002.

Ramachandran, S., and Rajesh, T. A.: Black carbon aerosol mass concentrations over Ahmedabad, an urban location in western India: comparison with urban sites in Asia, Europe, Canada, and the United States, J. Geophys. Res., 112, D06211, doi:10.1029/2006JD007488, 2007.

Ramanathan, V., Chung, C., Kim, D., Bettge, T., Buja, L., Kiehl, J. T., Washington, W. M., Fu, Q., Sikka, D. R., and Wild, M.: Atmospheric brown clouds: impacts on South Asian climate and hydrological cycle, P. Nantl. Acad. Sci. USA, 102, 5326-5333, doi:10.1073/pnas.0500656102, 2005.

Ramanathan, V., and Carmichael, G.: Global and regional climate changes due to black carbon, Nature Geosci., 1, 221-227,

2008.

Ran, L., Deng, Z. Z., Wang, P. C., and Xia, X. A.: Black carbon and wavelength-dependent aerosol absorption in the North China Plain based on two-year aethalometer measurements, submitted, 2016.

Ryerson, T. B., Andrews, A. E., Angevine, W. M., Bates, T. S., Brock, C. A., Cairns, B., Cohen, R. C., Cooper, O. R., de Gouw, J. A., Fehsenfeld, F. C., Ferrare, R. A., Fischer, M. L., Flagan, R. C., Goldstein, A. H., Hair, J. W., Hardesty, R. M., Hostetler, C. A., Jimenez, J. L., Langford, A. O., McCauley, E., McKeen, S. A., Molina, L. T., Nenes, A., Oltmans, S. J., Parrish, D. D., Pederson, J. R., Pierce, R. B., Prather, K., Quinn, P. K., Seinfeld, J. H., Senff, C. J., Sorooshian, A., Stutz, J., Surratt, J. D., Trainer, M., Volkamer, R., Williams, E. J., and Wofsy, S. C.: The 2010 California Research at the Nexus of Air Quality and Climate Change (CalNex) field study, J. Geophys. Res., 118, 5830-5866, doi:10.1002/jgrd.50331, 2013.

Safai, P. D., Raju, M. P., Maheshkumar, R. S., Kulkarni, J. R., Rao, P. S. P., and Devara, P. C. S.: Vertical profiles of black carbon aerosols over the urban locations in South India, Sci. Total Environ., 431, 323-331, doi:10.1016/j.scitotenv.2012.05.058, 2012.

Samset, B. H., Myhre, G., Schulz, M., Balkanski, Y., Bauer, S., Berntsen, T. K., Bian, H., Bellouin, N., Diehl, T., Easter, R. C., Ghan, S. J., Iversen, T., Kinne, S., Kirkevåg, A., Lamarque, J. F., Lin, G., Liu, X., Penner, J. E., Seland, Ø., Skeie, R. B., Stier, P., Takemura, T., Tsigaridis, K., and Zhang, K.: Black carbon vertical profiles strongly affect its radiative forcing uncertainty, Atmos. Chem. Phys., 13, 2423-2434, doi:10.5194/acp-13-2423-2013, 2013.

Schmid, O., Artaxo, P., Arnott,W. P., Chand, D., Gatti, L. V., Frank, G. P., Hoffer, A., Schnaiter, M., and Andreae, M. O.: Spectral light absorption by ambient aerosols influenced by biomass burning in the Amazon Basin. I: comparison and field calibration of absorption measurement techniques, Atmos. Chem. Phys., 6, 3443-3462, doi:10.5194/acp-6-3443-2006, 2006.

Seibert, P., Beyrich, F., Gryning, S. E., Joffre, S., Rasmussen, A., and Tercier, P.: Review and intercomparison of operational methods for the determination of the mixing height, Atmos. Environ., 34. 1001-1027, doi:10.1016/S1352-2310(99)00349-0, 2000.

Shao, M., Tang, X. Y., Zhang, Y. H., and Li, W. J.: City clusters in China: air and surface water pollution, Front. Ecol. Environ., 4, 353-361, doi:10.1890/1540-9295(2006)004[0353:CCICAA]2.0.CO;2, 2006.

Stier, P., Seinfeld, J. H., Kinne, S., and Boucher, O.: Aerosol absorption and radiative forcing, Atmos. Chem. Phys., 7, 5237-5261, doi:10.5194/acp-7-5237-2007, 2007.

Streets, D. G., Gupta, S., Waldhoff, S. T., Wang, M. Q., Bond, T. C., and Bo, Y. Y.: Black carbon emissions in China, Atmos. Environ., 35, 4281-4296, doi:10.1016/S1352-2310(01)00179-0, 2001.

Tripathi, S. N., Dey, S., Satheesh, S. K., Lal, S., and Venkataramani, S.: Enhanced layer of black carbon in a north Indian industrial Indian city, Geophys. Res. Lett., 32, L12802, doi:10.1029/2005GL022564, 2005.

Tripathi, S. N., Srivastava, A. K., Dey, S., Satheesh, S. K., Krishnamoorthy, K.: The vertical profile off atmospheric heating rate of black carbon aerosols at Kanpur in northern India, Atmos. Environ., 41, 6909-6915, doi:10.1016/j.atmosenv.2007.06.032, 2007.

Weingartner, E., Saathoff, H., Schnaiter, M., Streit, N., Bitnar, B., and Baltensperger, U.: Absorption of light by soot particles: determination of the absorption coefficient by means of aethalometers, J. Aerosol Sci., 34, 1445-1463, doi:10.1016/S0021-8502(03)00359-8, 2003.

Xu, W. Y., Zhao, C. S., Ran, L., Deng, Z. Z., Liu, P. F., Ma, N., Lin, W. L., Xu, X. B., Yan, P., He, X., Yu, J., Liang, W. D., and Chen, L. L.: Characteristics of pollutants and their correlation to meteorological conditions at a suburban site in the North China Plain, Atmos. Chem. Phys., 11, 4353-4369, doi:10.5194/acp-11-4353-2011, 2011.

Yu, T. W.: Determining height of the nocturnal boundary layer, J. Appl. Meteorol., 17, 28-33, 1978.

Yu, H. B., Liu, S. C., and Dickinson, R. E.: Radiative effects of aerosols on the evolution of the atmospheric boundary layer, J. Geophys. Res., 107, D12, doi:4142, 10.1029/2001JD000754, 2002.

Zarzycki, C. M. and Bond, T. C.: How much can the vertical distribution of black carbon affect its global direct radiative forcing?, Geophys. Res. Lett., 37, L20807, doi:10.1029/2010gl044555, 2010.

Zhao, D. L., Tie, X. X., Gao, Y., Zhang, Q., Tan, H. J., Bi, K., Jin, Y. L., and Chen, P. F.: In-situ aircraft measurements of the vertical distribution of black carbon in the lower troposphere of beijing, china, in the Spring and Summer Time, Atmos., 6, 713-731; doi:10.3390/atmos6050713, 2015.

Zhang, D. L., Chen, B., Yamada, M., Niu, H. Y., Wang, B., Iwasaka, Y., and Shi, G. Y.: Elevated soot layer in polluted urban atmosphere: a case study in Beijing, J. Meteorol. Soc. Japan, 90, 361-375, doi:10.2151/jmsj.2012-302, 2012.

Atmos. Chem. Phys. Discuss., doi:10.5194/acp-2016-219, 2016
Manuscript under review for journal Atmos. Chem. Phys.
Published: 18 April 2016

Atmospheric Chemistry and Physics Discussions

Table 1 A statistical summary of the field campaign and the meteorology. H_{max} denotes the maximum height reached by the tethered balloon. T_{10m}, RH_{10m}, and WS_{10m} indicated temperature, relative humidity, and wind speed within 10 m near the surface, in the form of average value±standard deviation. WD_{10m} represents frequently encountered wind direction. The last column gives the weather that mostly occurred during each period.

Periods	Profiles	H_{max} (km)	T_{10m} (°C)	RH_{10m} (%)	WS_{10m} (m s^{-1})	WD_{10m}	Weather
06:00-09:00	23	0.28~0.92	25.3±0.8	62.7±3.2	2.9±1.3	Southwest	Cloudy
09:00-12:00	20	0.32~1.06	26.0±1.5	61.0±3.4	2.6±1.1	Southwest	Cloudy
12:00-15:00	4	0.84~1.14	28.7±2.3	55.9±5.0	2.2±1.4	Southeast	Fine
15:00-18:00	6	1.04~1.08	28.5±2.4	58.7±4.6	2.1±1.1	Southeast	Fine
18:00-21:00	14	0.26~1.16	29.1±2.2	45.0±3.3	1.8±0.8	Southwest	Fine

Atmos. Chem. Phys. Discuss., doi:10.5194/acp-2016-219, 2016
Manuscript under review for journal Atmos. Chem. Phys.
Published: 18 April 2016

Atmospheric Chemistry and Physics Discussions

Table 2 Statistical parameters for BC vertical profiles measured during different periods. Notations for the parameters have been given in the text.

Parameters	06:00-09:00 23 Profiles	09:00-12:00 20 Profiles	12:00-15:00 4 Profiles	15:00-18:00 6 Profiles	18:00-21:00 14 Profiles
H_m (km)	0.08~0.29	0.18~0.87	0.43~1.14	0.69~1.08	0.19~0.25
H_e (km)	0.05±0.04	0.05±0.03			
C_m (μg m^{-3})	3.1~14.49 (6.61±2.93)	2.56~5.80 (4.42±1.11)	1.12~6.15 (3.77±2.06)	2.04~4.11 (3.05±0.86)	
C_f (μg m^{-3})	0.46~3.14 (1.67±0.95)	0.41~2.51 (1. 77±0.75)			0.36~2.83 (1.36±1.12)

Atmos. Chem. Phys. Discuss., doi:10.5194/acp-2016-219, 2016
Manuscript under review for journal Atmos. Chem. Phys.
Published: 18 April 2016

Atmospheric Chemistry and Physics Discussions

Table 3 Measurements of BC vertical distributions in different regions. m_{BC} is the range and/or average value±standard deviation of BC mass concentrations, depending upon what is available in the literature. Height specifies how m_{BC} is obtained.

Locations	Type	Period	Method	m_{BC} (μg m^{-3})	Height	References
Los Angeles Basin, USA	Mixture	May 2010	Aircraft, SP2*	0.01~0.53	0.3 km	Metcalf et al., 2012
				0.03±0.05	FT	
Milan, Italy	Urban	Feb. 2010	Tethered balloon, AE-51	7.57 ± 1.28	ML	Ferrero et al., 2014
				2.03 ± 0.34	FT	
Multi-cities, India	Urban	Jun. 2005	Aircraft, AE-42, AE-21	1.50~7.50	PBL	Safai et al., 2012 and references therein
Beijing, China	Urban	May-Jun. 2012	Aircraft, SP2	0.24~4.02	PBL	Zhao et al., 2015
Shanghai, China	Urban	Dec. 2013	Tethered balloon, AE-31	3.20~7.30	0-1 km	Li et al., 2015
Central NCP, China	Semirural	Jun.-Jul. 2014	Tethered balloon, AE-51	1.12~14.49 (5.16±2.49)	ML	This study
				0.36~3.14 (1.61±0.94)	FT	

* SP2: Single Particle Soot Photometer

Atmos. Chem. Phys. Discuss., doi:10.5194/acp-2016-219, 2016
Manuscript under review for journal Atmos. Chem. Phys.
Published: 18 April 2016

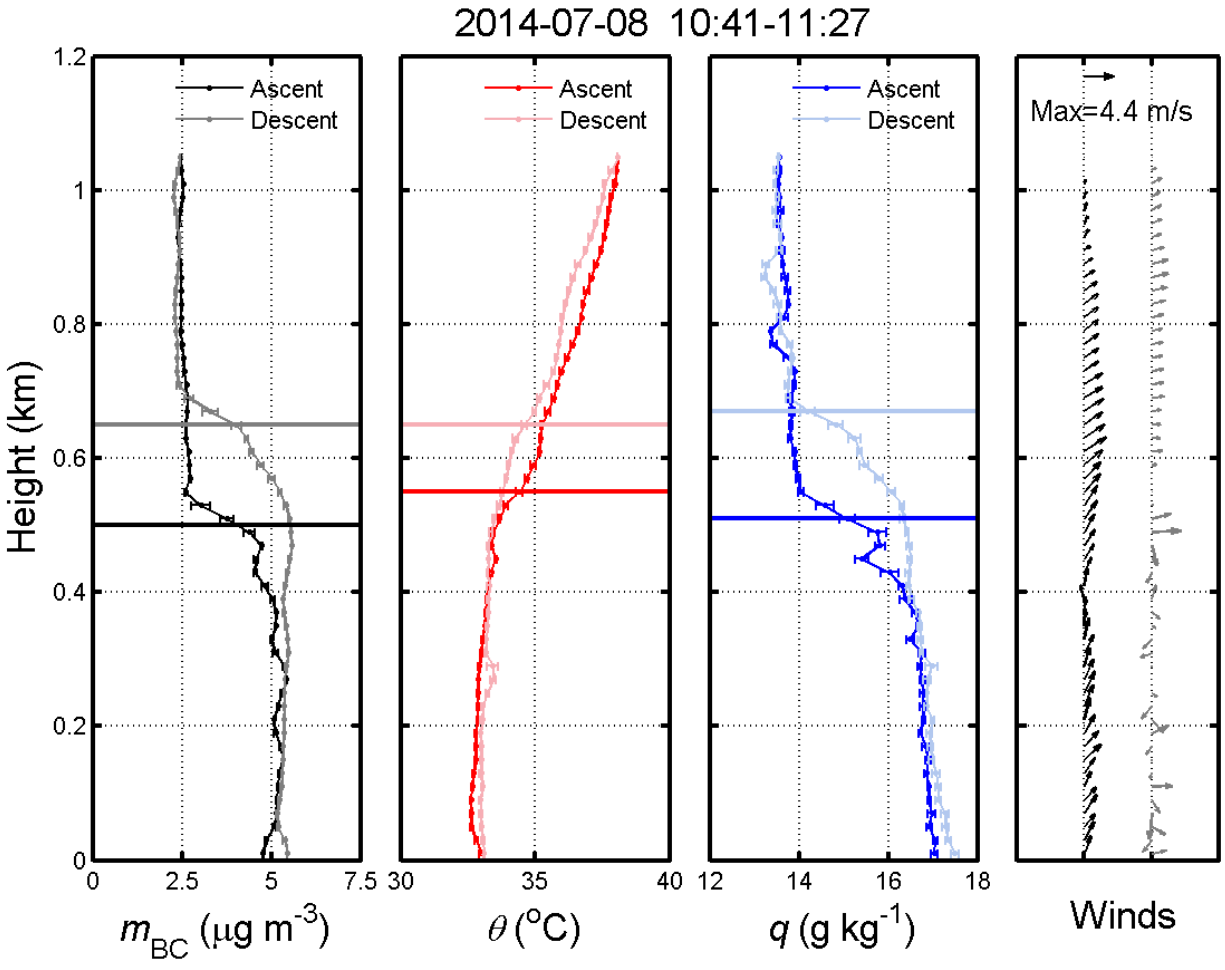

Figure 1. Vertical profiles of BC mass concentrations (m_{BC}), potential temperature (θ), specific humidity (q) and winds on July 8, 2014 (10:41-11:27 LT). Profiles measured during the ascent are displayed in dark colors, while the descent in light colors. Dots indicate 20-m averaged data, with standard deviations in error bars. Heights of the mixing layer (ML) estimated from vertical profiles are given in horizontal lines. Arrows show vector mean horizontal winds, with northerly winds indicated by downward arrows. The wind vector for the maximum wind speed is marked with the text.

Atmos. Chem. Phys. Discuss., doi:10.5194/acp-2016-219, 2016
Manuscript under review for journal Atmos. Chem. Phys.
Published: 18 April 2016

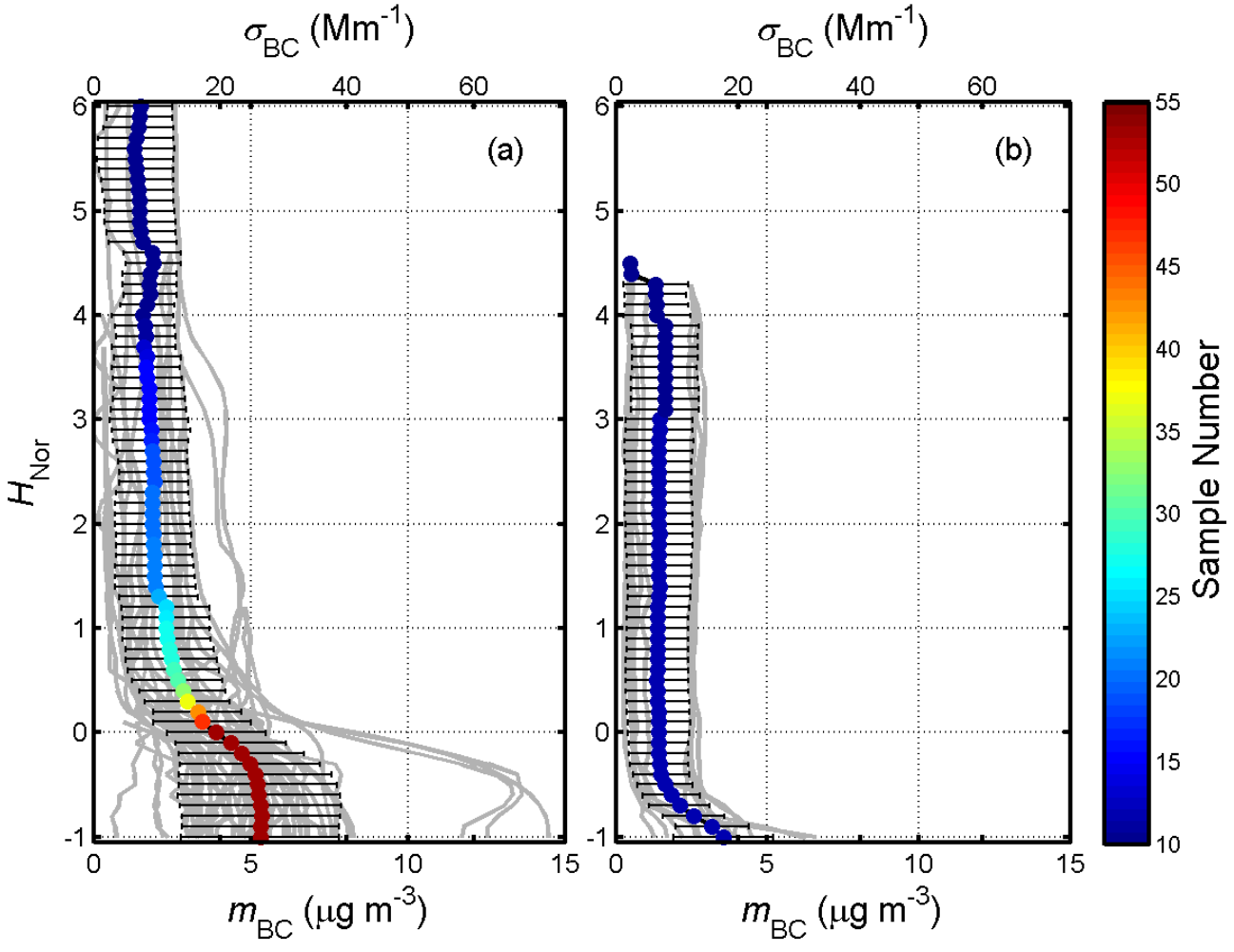

Figure 2. Vertical distributions of m_{BC} (bottom axis) and σ_{BC} (top axis) along the normalized height H_{Nor} (a) in the daytime and (b) in the evening during the field campaign (grey lines). The average profile is shown in black line, with error bars to represent standard deviations. Average values are indicated by dots, with the color to show the number of samples at each layer.

Atmos. Chem. Phys. Discuss., doi:10.5194/acp-2016-219, 2016
Manuscript under review for journal Atmos. Chem. Phys.
Published: 18 April 2016

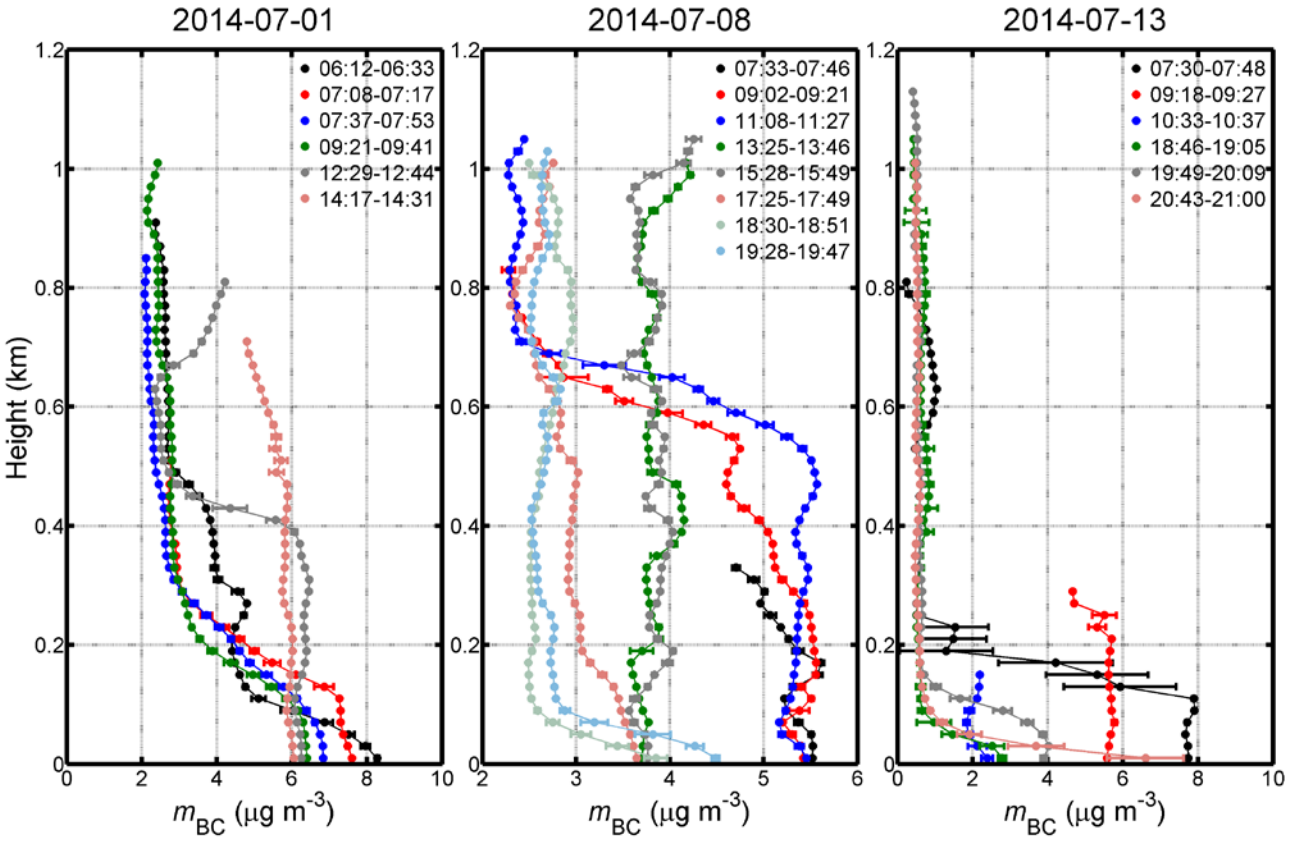

Figure 3. Vertical distributions of BC separately displayed for July 1, 8, and 13. Profiles collected at different time are shown in different colors. As in Fig. 1, dots represent 20-m averaged m_{BC}, with standard deviations given in error bars.

Atmos. Chem. Phys. Discuss., doi:10.5194/acp-2016-219, 2016
Manuscript under review for journal Atmos. Chem. Phys.
Published: 18 April 2016

Atmospheric Chemistry and Physics Discussions

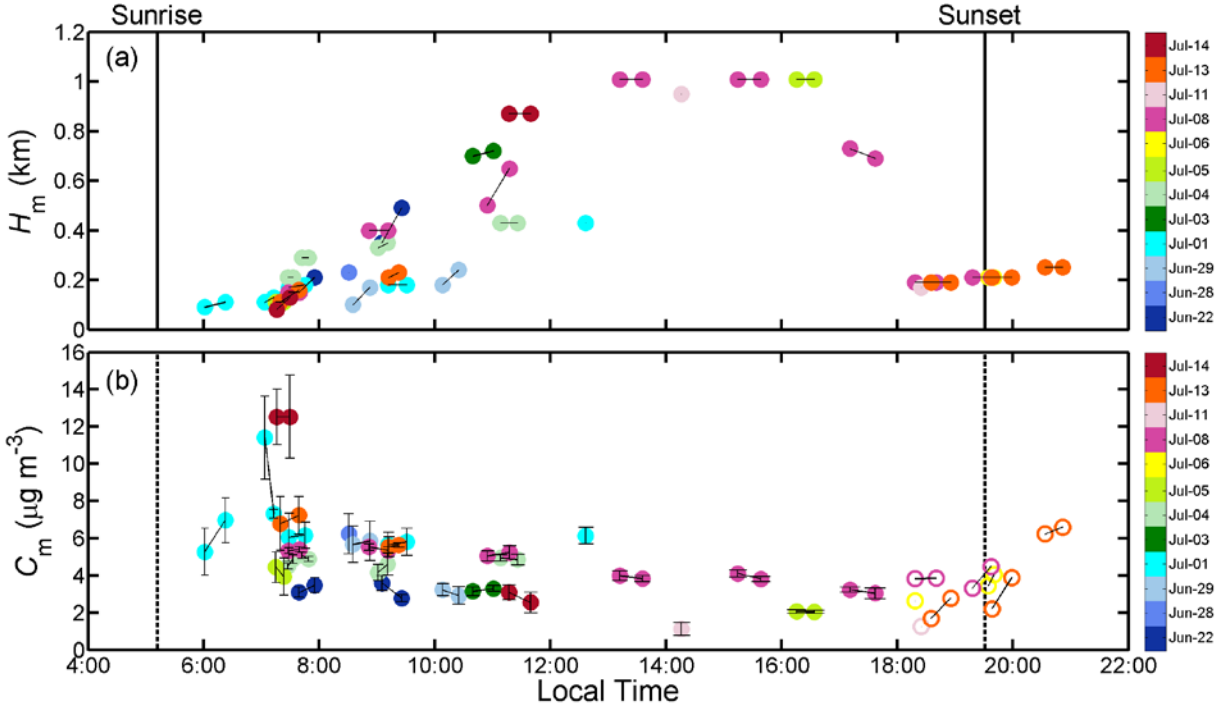

Figure 4. (a) H_m identified from BC vertical profiles in the selected dataset. Measurements made on different days are marked by dots in different colors. H_m from the ascent and descent of one launch are connected by black lines. (b) Average m_{BC} within the ML (C_m) during the daytime (before 18:00 LT) are marked by solid dots. Average m_{BC} within 20 m near the surface in the evening are marked by open dots.